Research Article Vol. 31, No. 19 / 11 Sep 2023 / Optics Express 30340
Optics EXPRESS

High-precision turning and ultra-smooth direct polishing of aluminum alloy mirrors

PENG SONG,[1] CHAO YANG,[1,*] YANG BAI,[2,3] JIAWEN DING,[1] JIE GUO,[1] CHUANG LI,[1] YUXUAN WANG,[1] AND CHANGXI XUE[1]

[1]*Changchun University of Science and Technology, School of Optoelectronic Engineering, Department of Optical Engineering, Chang Chun, Ji Lin 13022, China*
[2]*Changchun Institute of Optics, Fine Mechanics and Physics, Chinese Academy of Sciences, Chang Chun, Ji Lin 130033, China*
[3]*baiyang5406@sina.com*
[*]*yangchaoby@sina.com*

Abstract: Due to the high surface roughness requirements of aluminum alloy mirrors used in the visible light band, there are still great challenges in single point diamond turning of high-surface quality aluminum alloy mirrors. In this paper, a processing method for aluminum alloy mirrors is proposed. Based on single point diamond turning technology, the prediction model of aluminum alloy surface roughness was established. The mapping relationship between the surface roughness of the aluminum alloy mirror and each turning parameter was obtained, and the maximum possible surface quality was achieved. On the basis of the turning results, the method of small tool polishing was used to remove the turning texture generated by the copy effect of the tool arc radius, suppress errors of the medium and high-frequency, and reduce the surface roughness. The single abrasive removal efficiency model was established and mechanical removal in the polishing process was analyzed. Combined with the chemical action in the polishing process, two types of polishing liquid—acidic and neutral, were prepared and analyzed. The optimal polishing parameters were obtained through multiple single-factor experiments. On the basis of this, the surface roughness of the aluminum alloy after turning was optimized. The results show that the value was reduced from 4.811 to 1.482 nm, an increase of 69.2%. This method can effectively improve the machining accuracy of aluminum alloy mirrors and provide an important process guarantee for the application of aluminum alloy materials in visible-light systems.

1. Introduction

Aluminum mirrors have been widely used in high-performance telescopes, guidance, and navigation [1–3]. The difficult polishing characteristics of aluminum alloy materials challenge their applications in visible light [4]. The existing polishing technologies, such as magnetorheological polishing (MRF), ion beam polishing (IBF), and other processing methods, face some unavoidable problems in the application process. The MRF will remain small-scale ripples on the machined surface, resulting in intermediate-frequency errors in the mirror. At the same time, there is an oxide layer on the surface after MRF processing, which results in insufficient reflectivity [5,6]. IBF must be processed under vacuum conditions, and the sputtering effect leads to a low material removal rate, long processing cycles, and high cost, so it cannot be widely used [7]. Compared with these methods, the combination of single point diamond turning and small tool polishing is expected to become one of the most promising methods for ultra-smooth machining of aluminum alloy reflection.

The single point diamond turning (SPDT) technology is one of the most effective methods for the rapid processing of high-precision optical components [8,9]. In the study of SPDT processing, T. Sugano *et al.* first analyzed the influence of diamond turning parameters on the processing

#495779 https://doi.org/10.1364/OE.495779
Journal © 2023 Received 16 May 2023; revised 13 Aug 2023; accepted 15 Aug 2023; published 30 Aug 2023

Optics EXPRESS

results of aluminum alloy mirrors [10]; Sharma *et al.* analyzed the effect of tool wear on the machined surface during diamond turning [11]; Zhang *et al.* studied the dynamic characteristics of forced vibration caused by the unbalance of the diamond turning spindle and its influence on surface generation [12]. Although these studies have made some progress in single point diamond processing, the turning texture generated by the copy effect of tool arc radius of diamond turning always limits the applications of aluminum alloy mirrors in visible light systems.

Furthermore, small tool polishing is increasingly being used to process high-precision aluminum alloy mirrors. Small tool polishing has the advantages of a high removal rate, various sizes of polishing discs, and excellent suppression of medium and high frequency errors [13]. In the field of small tool polishing of aluminum alloy materials, most researchers pay attention to the polishing process and polishing results. Cho *et al.* studied the influence of polishing pad and polishing pressure on polishing results, and improved the processing efficiency and surface roughness of chemical mechanical polishing by optimizing the processing technology [14]. Yoomin *et al.* studied the effect of the pH value of the slurry on the polishing efficiency during the chemical mechanical polishing of aluminum alloy materials. It was concluded that the weak acid with a pH value of approximately 4 had a higher removal efficiency for aluminum alloy materials [15]. Du *et al.* conducted four polishing iterations on an aluminum alloy mirror with an aperture of 100 mm and obtained a machining result with a surface roughness *Ra* of 3.7 nm [16]. Zhao *et al.* suppressed the surface crystallization of the aluminum alloy mirror during the polishing process and obtained an aluminum alloy mirror with a surface roughness *Ra* of 2.78 nm through actual processing [17]. However, the proposed optimization met the expectations is still limited by its low processing efficiency and low surface quality of aluminum alloy mirrors.

Therefore, in this paper, we combined the advantages of single point diamond turning and small tool polishing to improve the processing quality while shortening the processing cycle and obtaining aluminum alloy mirrors that can be applied to the visible light band. First, single point diamond turning is used to rapidly process aluminum alloy mirrors to obtain nanoscale surface roughness. Then, two types of acidic and neutral small tool polishing liquids were prepared to polish the aluminum alloy reflector quickly and uniformly. Finally, by optimizing the processing parameters, the ultra-smooth surface that can be directly applied to the reflective optical system was obtained. The method proposed in this paper realizes the ultra-smooth processing of aluminum alloy mirrors, while ensuring the surface quality of the aluminum alloy mirror, it is beneficial to improve the processing efficiency, reduce the processing cost, and realize its wide application in the visible light system.

2. SPDT rapid processing of aluminum alloy mirror

The SPDT technology device is shown in Fig. 1. In the experimental machining process of the aluminum alloy mirror, the workpiece rotates at high speed with the rotation of C-axis. The diamond tool is used as the cutting tool to move along the Z-axis direction. At the same time, the workpiece feeds along the X-axis direction, and the XZC three-axis linkage realizes the ultra-precision turning of the aluminum alloy mirror.

In SPDT technology, because the front end of the diamond tool is a small radius surface, the lateral movement of the tool on the surface of the part will copy the tool arc radius. Under ideal conditions, the surface morphology after single point diamond turning is shown in Fig. 2 [18].

As shown in Fig. 2, according to the characteristics of the single point diamond turning, the turning texture generated by the copy effect of the tool arc radius is the main reason affecting the surface roughness during the machining process. The turning texture is mainly related to the turning parameters. The surface roughness of the turning texture during diamond turning can be predicted by simulation.

Optics EXPRESS

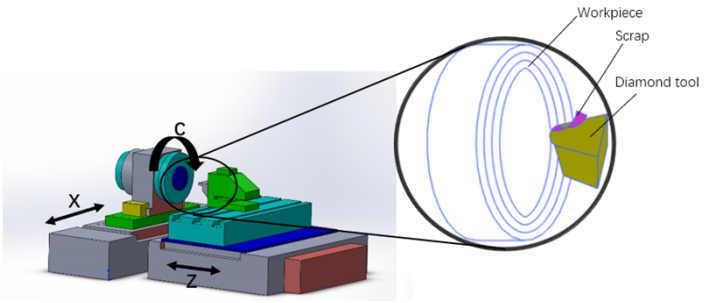

Fig. 1. Single point diamond turning diagram.

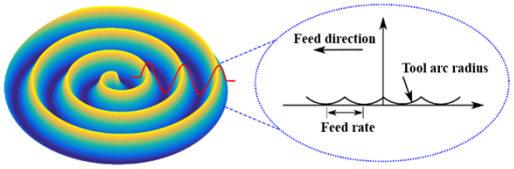

(a)

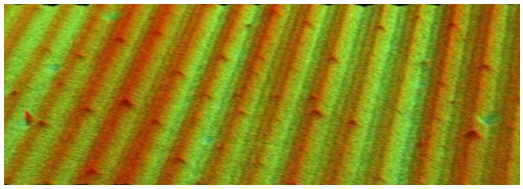

(b)

Fig. 2. Turning surface morphology diagram. (a) Theoretical surface profile caused by copy effect of tool arc radius; (b) The phenomenon of copy effect of tool arc radius in the actual surface profile.

2.1. *Prediction model of surface roughness caused by the copy effect of the radius of the tool arc*

The surface profile height difference of the optical element processed by SPDT in the ideal state is expressed as:

$$R_t = r_t - \sqrt{r_t^2 - \frac{f^2}{2N}} \tag{1}$$

where R_t represents the theoretical surface roughness, r_t represents the radius of the tool arc, f represents feed on the X-axis, and N represents speed on the C-axis, respectively.

In the process of diamond turning, the copy effect caused by the radius of the tool arc is the main factor that affects the surface roughness of optical components. The whole copy effect of the tool arc radius can be regarded as the superposition of the copy effect on the tool arc radius of each revolution. Thus, the arithmetic mean value of the surface roughness *Ra* can be obtained as follows:

$$R_a = \frac{N}{f}\int_0^{\frac{f}{N}} r_t - \sqrt{r_t^2 - x^2}dx \tag{2}$$

Optics EXPRESS

The simulation of the aluminum alloy turning process using the ABAQUS finite element simulation software is shown in Fig. 3. The material properties of the aluminum alloy are shown in Table 1 [19].

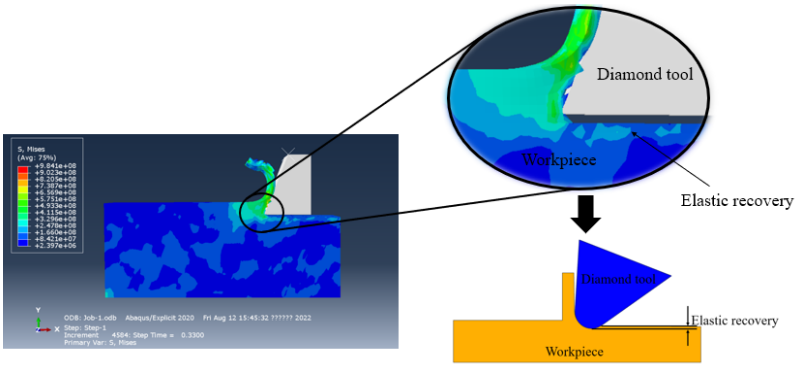

Fig. 3. Turning process of the aluminum alloy mirror.

Table 1. Material property parameters of RSA-6061 aluminum alloy

Density/(g/cm^3)	Elastic Mod/GPa	Yield strength/MPa	CTE, linear/(1/°C)	Elongation /%
2.7	69	315	0.0000230	16

It is shown that when the tool is in contact with the workpiece, the plastic deformation of the workpiece removes the material and elastic deformation occurs at the same time [20]. Therefore, the surface roughness of the aluminum alloy mirror is affected not only by the copy effect of the tool arc radius in the actual machining process, but it is also affected by elastic recovery. Elastic recovery is a severe deformation in the contact between the material and the tool during the cutting process. After the tool and the workpiece are separated, the elastic deformation of the material is partially restored, and the plastic deformation is retained. As shown in Fig. 3, to release stress, the material rebounds in the opposite direction of the extrusion, so the elastic rebound will reduce the surface roughness. On the basis of the above analysis, the surface roughness of the aluminum alloy mirror is expressed as follows:

$$R_{th} = R_t - s \tag{3}$$

$$R_{ah} = \frac{N}{f}\int_0^{\frac{f}{N}} \left(r_t - \sqrt{r_t^2 - x^2} - s\right) dx \tag{4}$$

where R_{th} represents the theoretical surface roughness; R_{ah} represents the arithmetic mean of the theoretical surface roughness; s denotes the elastic recovery of the material.

In the ultra-precision machining process of aluminum alloy mirrors, the elastic recovery of the material affects the surface roughness. According to the elastic recovery model of the SPDT machining process [21], elastic recovery in the ultra-precision machining process can be expressed as follows:

$$s = (1 - \varepsilon_p)h_{\min} \tag{5}$$

where ε_p represents the plastic deformation of the workpiece surface, h_{min} represents the minimum undeformed cutting thickness, that is expressed as $h_{min} = cr_a$, c is a coefficient of 0.3 to 0.4, which taken 0.34 in this paper, r_a is the radius of cutting edge.

Optics EXPRESS

Therefore, the surface roughness of the aluminum alloy mirror can be expressed as follows:

$$R_{th} = r_t - \sqrt{r_t^2 - \frac{f^2}{2N}} - 0.34(1-\varepsilon_p)r_a \tag{6}$$

$$R_{ah} = \frac{N}{f}\int_0^{\frac{f}{N}} \left(r_t - \sqrt{r_t^2 - x^2} - 0.34(1-\varepsilon_p)r_a\right) dx \tag{7}$$

Based on the above theories, the surface roughness of aluminum alloy mirrors is analyzed by numerical simulation. According to the relationship between the surface roughness of the aluminum alloy mirror and the turning parameters obtained by Eq. (6) and Eq. (7), the surface roughness changes with the variation of tool radius, feed speed, and spindle speed. The radius of the tool arc is selected between 0.25~0.75 mm, the feed speed is between 0.5~5.5 mm/min, and the spindle speed is between 1000~2000RPM. The relationship between the coupling of any above two factors and the surface roughness is numerically simulated by the control variables method. The simulation results are shown in Fig. 4(a), (b), and (c).

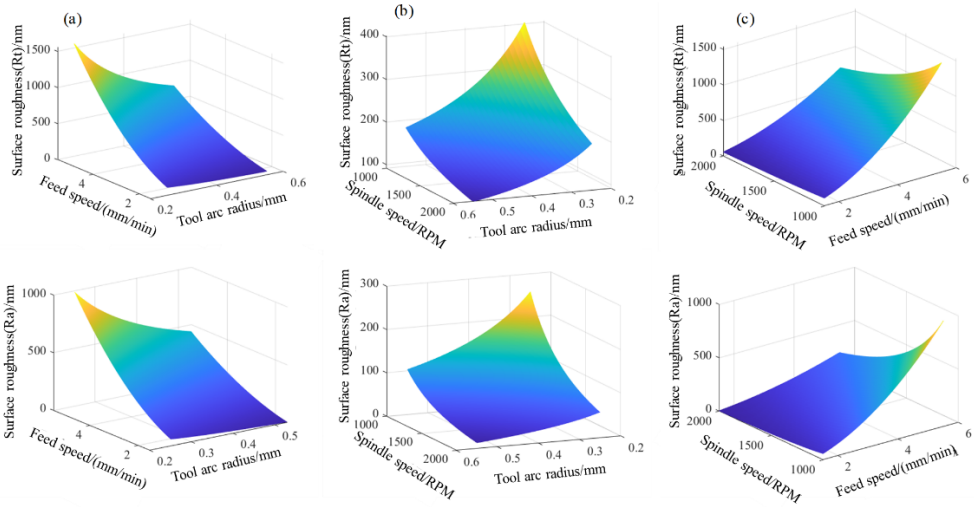

Fig. 4. Relationship between turning parameters and surface roughness *Rt* and *Ra*. (a) Tool radius - feed speed; (b)Tool radius - spindle speed; (c) Feed speed - spindle speed.

Fig. 4 shows the influence of any two-factors coupling on surface roughness. Fig. 4(a) shows the influence of the coupling of the tool radius and feed speed on the surface roughness when the spindle speed is constant. The X-axis represents the radius of the tool, the Y-axis represents the feed speed, and the Z-axis represents the surface roughness, respectively. It can be seen that when the tool radius increases, the condition for the feed speed to decrease synchronously is small, and the surface roughness decreases all the time. The slope of the direction of the feeding speed is greater than the direction of the radius of the tool, indicating that the influence of the feeding speed on the surface roughness is greater than the influence of the tool radius on the surface roughness. Fig. 4(b) shows the influence of the coupling of the tool arc radius and the spindle speed on the surface roughness when the feed speed is constant. The X-axis and the Y-axis represent the spindle speed and the tool arc radius, respectively, and the Z-axis represents the surface roughness. When the spindle speed and tool arc radius increase synchronously, surface roughness decreases. Fig. 4(c) shows the influence of the coupling of spindle speed and feed speed on the surface roughness when the radius of the tool arc is constant. The X-axis, Y-axis, and Z-axis represent the spindle speed, feed speed, and surface roughness, respectively. The

Optics EXPRESS

numerical simulation results show that the surface roughness decreases when the ratio of feed speed to spindle speed decreases.

In order to further explore the influence of a single factor on surface roughness, the numerical simulation of Eq. (6) and Eq. (7) is carried out. Under the premise of controlling other factors, the surface roughness of a single factor is simulated. The simulation results are shown in Fig. 5(a), (b), and (c).

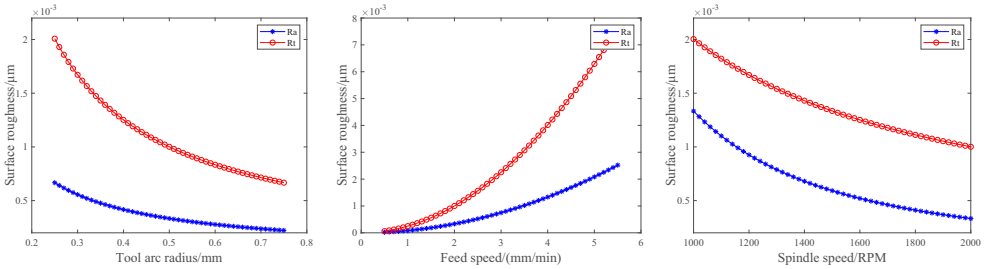

Fig. 5. Effect of the machining parameters on surface roughness. (a) Effect of the radius of the tool arc on surface roughness; (b) Effect of the feed speed on surface roughness; (c) The influence of the spindle speed on surface roughness.

Fig. 5 shows the influence of a single factor on surface roughness, in which Fig. 5(a) represents the influence of the radius of the arc of the tool on the surface roughness when the spindle speed and feed speed are constant; Fig. 5(b) represents the influence of the feed speed on surface roughness when the radius of the arc of the tool and the spindle speed are constant. Fig. 5(c) represents the influence of spindle speed on surface roughness when the tool arc radius and feed speed are constant. According to the simulation results of Fig. 5 and the turning contour of Fig. 2, it can be concluded that from Fig. 5(a), with the increase of the tool arc radius, the peak-valley ratio between the lowest point and the highest point of the turning texture decreases, and the surface roughness value decreases. However, in the actual cutting process, when the cutting depth is constant, the greater the tool arc radius, the greater the radial cutting force. It leads to the vibration between the tool and the workpiece, resulting in unfavorable factors affecting the surface roughness. It can be seen from Fig. 5(b) that when the feed speed is reduced, the surface roughness value will reduce because the post-cutting trajectory will cut the highest point of the previous turning trajectory at the same time, so that the surface roughness value is reduced. However, in ultra-precision cutting, if the feed speed is too small, the machine tool is prone to low-speed crawling and other phenomena, which will increase the surface roughness. It is shown in Fig. 5(c) that when the spindle speed increases, the surface roughness will decrease. This is because in unit time, the feed speed is constant and the increase of the spindle speed leads to a decrease in the ratio of the feed speed to the spindle speed, that is, the feed speed per rotation decreases, thereby reducing the surface roughness. However, in actual processing, with increasing spindle speed, the relative vibration between the workpiece and the tool also increases, and the adverse factors that affect the surface quality of the processed surface also increase. Therefore, when the speed increases to a certain extent, the surface roughness decreases very slowly and even has an increasing trend.

In summary, in the single point diamond turning of optical components, the turning trajectory (including feed speed, spindle speed, and tool arc radius) and elastic recovery are the main reasons for the formation of surface roughness of optical components. In the actual machining process, the surface roughness of optical components can be improved by controlling the turning parameters. In this paper, it is necessary to use single point diamond turning to quickly obtain an aluminum alloy reflector with a surface roughness *Ra* value of less than 5 nm. The spindle speed

Optics EXPRESS

can be selected at 1500~2000RPM, the tool arc radius is 0.4~0.55 mm, and the feed speed is 1.5~2 mm/min.

2.2. Rapid processing experiment of aluminum alloy mirror

According to the analysis of the previous section, to quickly obtain a high-quality aluminum alloy mirror, the Precitech Nanoform 700 single point diamond lathe is used as the processing equipment to quickly process the RSA-6061 aluminum alloy plane mirror with a diameter of 150 mm. The specific processing parameters are shown in Table 2.

Table 2. Process parameters of SPDT

Parameters	Value
Tool arc radius	0.51mm
Feed rate	1.7 mm/min
Spindle speed	2000RPM
Depth of cut	0.2mm

The surface roughness of diamond-turned aluminum alloy plane mirror is detected by Zygo's New View 7200 white light interferometer. The machining process and detection results are shown in Fig. 6.

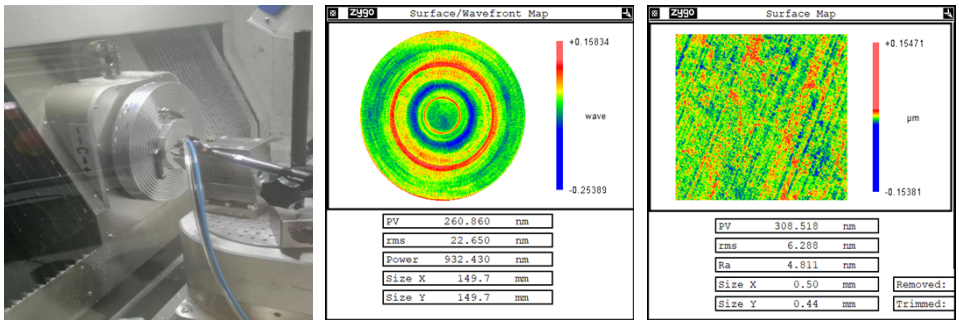

(a) (b) (c)

Fig. 6. SPDT machining process and results. (a) Machining process; (b) Surface profile test results; (c) Surface roughness test results.

It can be seen from Fig. 6(b) that the RMS of Surface profile accuracy after single point diamond turning is 22.65 nm. Fig. 6(c) shows that the surface roughness Ra of the aluminum alloy mirror is 4.811 nm. Although the surface roughness of the aluminum alloy plane mirror after diamond turning has reached the nanometer level, it is still possible to observe the copy distribution of the tool arc radius with different depths on its surface (turning texture). In the traditional diamond turning process, turning texture is inevitable, resulting in a large medium and high-frequency error of the aluminum alloy mirror. The aluminum alloy mirror with turning texture on the surface will produce obvious diffraction and scattering phenomena when it is directly applied to the visible light system, which will seriously affect the imaging quality and reflectivity, and even cannot be used. Therefore, it is necessary to suppress the medium and high-frequency errors of the diamond turning aluminum alloy mirror surface.

3. Small tool polishing to remove medium and high-frequency error

Small tool polishing is an atomic removal technology. The chemical reaction of the polishing slurry and the mechanical interaction of the abrasive are combined to remove the material. The

Optics EXPRESS

workpiece is fixed on the spindle, the polishing head and the polishing pad are driven by a servo motor with adjustable speed and the pressure is applied downward [22,23]. The polishing slurry removes surface defects by chemical action and then removes them through the mechanical interaction of the incoming abrasive to obtain an ultra-smooth surface, as shown in Fig. 7.

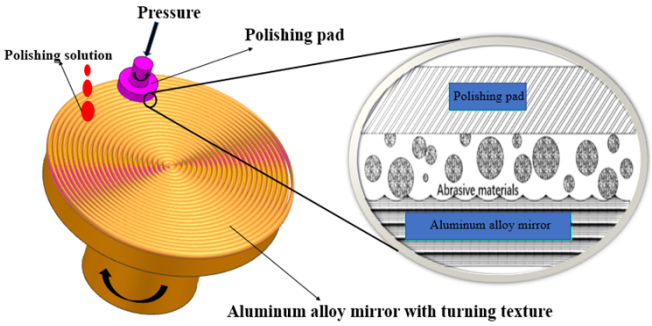

Fig. 7. Schematic diagram of small tool polishing.

In the small tool polishing removal mechanism, the chemical reaction corrodes the surface of the aluminum alloy mirror, which is convenient for subsequent mechanical removal. Mechanical action removes the surface after the chemical reaction. Chemical and mechanical effects play the same key role in material removal.

3.1. Mechanical action in polishing process

Polishing is the removal of a certain material on the surface of the workpiece to achieve the purpose of reducing the surface roughness. In the polishing process, the workpiece and the abrasive particles contact each other, resulting in wear. And the actual wear process is caused by the sliding friction of the abrasive particles embedded in the uneven polishing pad. During the polishing process, the abrasive particles flow through the surface peak, so that the valley value of the peak valley of the surface gradually decreases. The polished abrasive particles will continue to flow through the peak to remove material, and the peak-valley gap will gradually shrink. Finally, the workpiece surface will tend to be smooth at this position, thereby improving the quality of the workpiece surface. Therefore, the polished abrasive particles flow through the peaks and troughs of the surface, and the material is continuously removed to finally obtain a high-quality surface.

3.1.1. Mathematical modeling of the material removal function

In the polishing process, the abrasive particles pass through the surface of the workpiece, and the average depth of indentation can be approximated as the final roughness of the polished surface [24]. Fig. 8 shows the wear behavior of a single abrasive particle on the surface of an aluminum alloy mirror.

The volume of material removed by a single abrasive particle on the surface of the aluminum alloy is expressed as [25]:

$$M = K_t S_t V_t \tag{8}$$

where M represents the volume of removal of the material, K_t represents the wear constantly, S_t represents the cross-sectional area of wear on the surface of the aluminum alloy, and V_t represents the linear velocity of the abrasive particles during polishing.

Optics EXPRESS

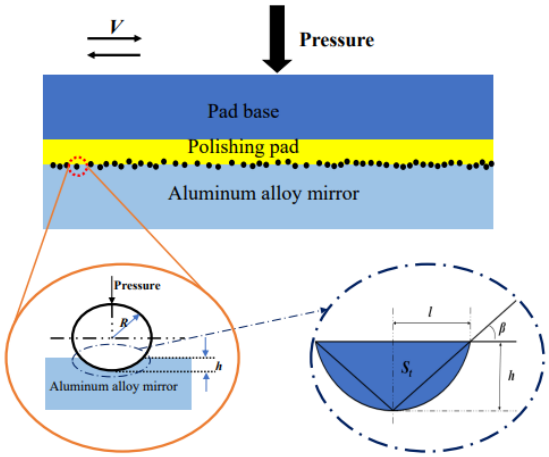

Fig. 8. The contact diagram of the abrasive grain and surface during the polishing process.

Through Rabinowicz's research [26], it can be concluded that the wear constant has the following relationship as:

$$K_t = \frac{3}{\pi}\tan\beta \tag{9}$$

where β is the cut-in angle of the abrasive particles pressed onto the surface of the aluminum alloy, as shown in Fig. 8. The specific value of the wear constant can be obtained by the following geometric relationship as:

$$\begin{cases} \tan\beta = \frac{h}{l} \\ l = \sqrt{R^2 - (R-h)^2} \end{cases} \tag{10}$$

where h represents the depth of the indentation, l represents the radius of the indentation, and R represents the abrasive radius. In the modeling process, $h \le R$ should be satisfied. Bring Eq. (10) into Eq. (9) yields that

$$K_t = \frac{3\sqrt{h}}{\pi\sqrt{2R-h}} \tag{11}$$

According to the geometric relationship in Fig. 8, the cross-sectional area of the material removed by a single abrasive grain has the following relationship, which is expressed as:

$$S_t = 2R^2\tan^{-1}\left(\frac{\sqrt{h}}{\sqrt{2R-h}}\right) - R\sqrt{h(2R-h)} + h\sqrt{h(2R-h)} \tag{12}$$

The volume of material removal of a single abrasive particle on the surface of the aluminum alloy can be obtained by bringing Eq. (11) and Eq. (12) into Eq. (8):

$$M = \frac{3\sqrt{h}}{\pi\sqrt{2R-h}}\left(2R^2\tan^{-1}\left(\frac{\sqrt{h}}{\sqrt{2R-h}}\right) - R\sqrt{h(2R-h)} + h\sqrt{h(2R-h)}\right)V_t \tag{13}$$

In the process of small tool polishing, the rotation speed of the polishing disc has the following relationship with the linear speed of a single abrasive polishing:

$$V_t = \pi d v \tag{14}$$

where v represents the rotational speed of the polishing disc; d denotes the diameter of the polishing disk.

Optics EXPRESS

Substituting Eq. (14) into Eq. (13) yields the following as:

$$M = \frac{3dv\sqrt{h}}{\sqrt{2R-h}}\left(2R^2\tan^{-1}\left(\frac{\sqrt{h}}{\sqrt{2R-h}}\right) - R\sqrt{h(2R-h)} + h\sqrt{h(2R-h)}\right) \tag{15}$$

According to Eq. (15), the material removal volume is related to the indentation depth, and the radius of the abrasive particle and the indentation depth have the following relationship as [27]:

$$F = 2\pi RHh \tag{16}$$

where F is the pressure and H is the hardness of the surface of the material.

Then, substituting Eq. (16) into Eq. (15), the removal volume has the following relationship with pressure and speed, which is shown as:

$$M' = \frac{3dv}{2R}\sqrt{\frac{F}{2\pi H}}\left(\begin{array}{l} 2R^2\tan^{-1}\left(\sqrt{\frac{F}{2\pi H}}\right) - R\sqrt{\frac{F}{4\pi RH}\left(2R-\frac{F}{4\pi RH}\right)} + \\ \frac{F}{4\pi RH}\sqrt{\frac{F}{4\pi RH}\left(2R-\frac{F}{4\pi RH}\right)} \end{array}\right) \tag{17}$$

3.1.2. Numerical simulation of material removal function

The volume of material removal in the small tool polishing process is the result of the accumulation of multiple abrasive grains. Therefore, in the simulation process, studying the surface removal of optical components by a single abrasive particle can predict mechanical removal.

The numerical simulation of Eq. (17) is carried out using the MATLAB software. The influence of linear velocity and pressure on the material removal volume per unit of time is discussed, respectively. The simulation results are shown in Fig. 9.

In Fig. 9(a), the abscissa represents the linear speed of polishing, and the ordinate represents the removal volume; the linear velocity is set to 0.1π~0.15π m/s respectively. When the feed pressure is 8×10^{-11}N, the abrasive size is set to 1μm, 2μm, 3μm, 4μm, and 5μm respectively. Additionally, when the abrasive particle size is 10μm, the pressure is set to 0.5×10^{-11}N, 1.5×10^{-10}N, 2.5×10^{-10}N, 3.5×10^{-10}N, and 4.5×10^{-10}N. In Fig. 9(a). It can be found that the material removal per unit of time is proportional to the linear velocity. When the abrasive particle diameter is constant and the pressure increases, the greater the pressure, the greater the material removal efficiency. This is because the greater the pressure, the greater the depth of the abrasive particles pressed into the polished material, resulting in an increase in the removal volume. When the polishing pressure is constant, the larger the diameter of the abrasive particle, the smaller the removal efficiency. This is because the depth of the large-diameter abrasive particles pressing into the polished material is smaller under the same pressure, while the depth of small-diameter abrasive particlepssing io the polished material is larger. In this case, when calculating the cross-sectional area of the abrasive particle removal material, the cross-sectional area of the small-diameter abrasive particle removal material is larger than the cross-sectional area of the large-diameter abrasive particle removal material, resulting in the removal efficiency of the small-diameter abrasive particle being greater than the removal efficiency of the large-diameter abrasive particle. But in the actual application process, the abrasive particles will move during the rotation of the polishing disc. With increasing rotational speed, the centrifugal force of the abrasive particles increases, resulting in a decrease in the concentration of the abrasive particles under the polishing disc, which leads to a decrease in the removal efficiency. In Fig. 9(b), the abscissa represents the polishing pressure and the ordinate represents the removal volume; the pressure is set to 0.5×10^{-10}~5×10^{-10}N, and the linear velocity is set to 0.1π m/s, 0.15π m/s, 0.2π m/s, 0.25π m/s, and 0.3π m/s respectively when the abrasive particle size is 10μm. In addition, when the online speed is set to 0.1π m/s, the abrasive size is set to 1μm, 2μm, 3μm, 4μm and 5μm respectively. In Fig. 9(b), it can be found that when the indentation depth is less than

Optics EXPRESS

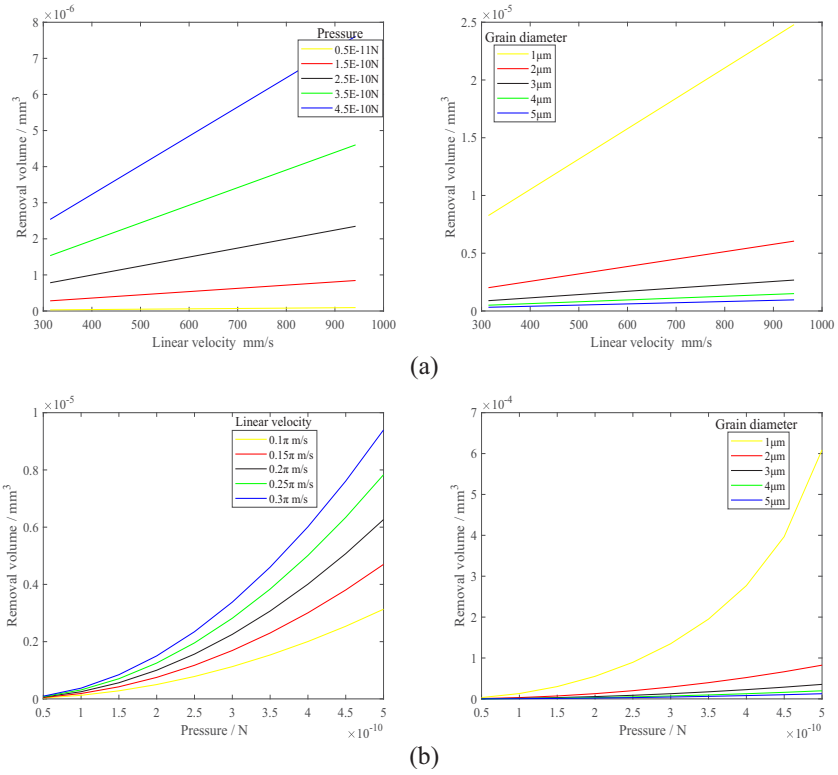

Fig. 9. Results of the material removal volume simulation. (a) The relationship between polishing line speed and removal volume; (b)The relationship between pressure and removal volume.

the abrasive radius, with the increase of pressure, the material removal efficiency will increase parabolically at any angular velocity and abrasive size. Therefore, the polishing efficiency can be improved by increasing the pressure. However, in the actual application process, excessive polishing pressure will cause scratches on the surface of the polished material and affect the polishing effect.

In summary, material removal efficiency is proportional to linear velocity and pressure during the polishing process. Therefore, to improve the polishing efficiency, the speed and pressure of the polishing disc can be appropriately increased.

3.2. Chemical action in the polishing process

The chemical action in the polishing process refers to chemical corrosion under a special condition. And the defects in the metal surface are removed by controlling the selective dissolution of the metal surface. Selective dissolution refers to the uneven dissolution of the polished surface due to the uneven geometric structure. The convex part dissolves more, while the concave part dissolves less, causing the final surface becomes flat and bright.

The polishing solution that reacts with aluminum alloy is usually an acidic solution or an alkaline solution. As a result of the strong corrosion of the alkaline solution, there will be a black film on the machined surface, which affects the effect of use. Therefore, the acidic polishing solution is prepared in this paper.

According to the chemical composition of RSA-6061 aluminum alloy shown in Table 3 [6], the chemical reaction process is obtained in Fig. 10.

Optics EXPRESS

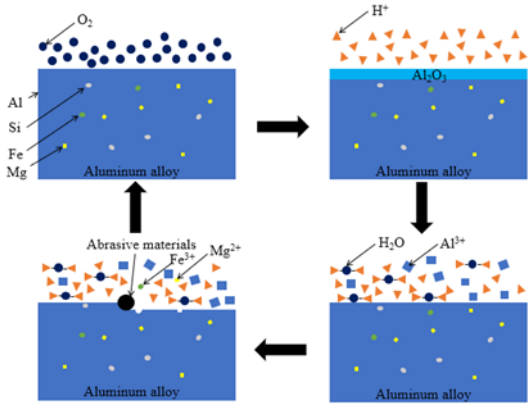

Fig. 10. Chemical reaction diagram of the aluminum alloy mirror polishing process.

Table 3. Chemical composition of RSA-6061

Name	Al	Mg	Fe	Si	Others
Contents %	97.35	1.0	0.3	0.6	0.75

As shown in Fig. 10, since the chemical properties of aluminum are very active, oxidation reactions can occur in the air to form oxides. Therefore, before the chemical reactions of *Al*, *Fe*, and *Mg* elements in acidic liquids, the alumina on the surface of the aluminum alloy undergo chemical reactions to form water-soluble compounds. The process is as follows:

$$Al_2O_3 + 6H^+ \rightarrow 3Al^{3+} + 3H_2O \tag{18}$$

After the surface Al_2O_3 is removed, the *Al*, *Fe*, and *Mg* elements in the RSA6061 aluminum alloy mirror will react with the acid to form a water-soluble compound. The process is as follows:

$$2Al + 6H^+ \rightarrow 2Al^{3+} + 3H_2 \uparrow \tag{19}$$

$$Mg + 2H^+ \rightarrow Mg^{2+} + H_2 \uparrow \tag{20}$$

$$2Fe + 6H^+ \rightarrow 2Fe^{3+} + 3H_2 \uparrow \tag{21}$$

From Eq. (18) to Eq. (21), it can be seen that the pH value of the polishing liquid can affect the polishing rate. The surface morphology of the aluminum alloy mirror after polishing in acidic polishing liquid and neutral polishing liquid is shown in Fig. 11. From Fig. 11(a), it shows that *Mg* and *Fe* elements in aluminum alloy will also react chemically under acidic conditions, resulting in pitting corrosion on the surface of polished optical elements and affecting the surface quality of optical elements. At the same time, the surface of a strong acid aluminum alloy with a pH value less than 4 is severely corroded. Therefore, the polishing solution should choose a weak acid with a pH value greater than or equal to 4. The chemical corrosion decreases with the increase in the pH value and the polishing removal efficiency decreases. From Fig. 11(b), it is shown that the chemical reaction is weakened and the physical removal is enhanced in the neutral polishing liquid with pH value of 7. Although the removal efficiency is slow during the polishing process, the surface quality of the polished aluminum alloy mirror is better. In summary, in this paper, an efficient acid polishing liquid with a pH value of 4 for rapid removal of turning texture and a neutral polishing liquid with a pH value of 7 are prepared improve the surface quality of aluminum alloy reflectors. The aluminum alloy reflector is ultra-precision polished by the combination of two polishing liquids.

Optics EXPRESS

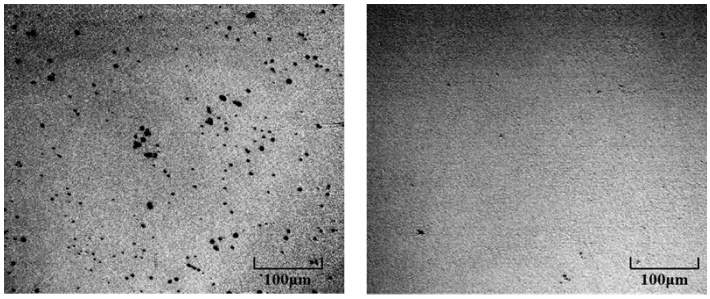

(a) (b)

Fig. 11. The surface of aluminum alloy after polishing with different polishing liquid. (a) Acidic polishing liquid; (b) Neutral polishing liquid.

3.3. Fast super-smooth polishing experiment of aluminum alloy mirror

3.3.1. Optimization of experimental parameters

Through the analysis of material removal efficiency, the relationship between linear velocity, pressure, and polishing efficiency can be obtained. In the actual polishing process, the pressure of a single abrasive particle is not calculated directly. Therefore, based on the numerical simulation, it is necessary to carry out specific experiments to determine the best polishing parameters. In addition to considering the polishing efficiency, the surface roughness of the processed optical components is more important.

During the polishing process, the chemical and mechanical effects of material removal during the polishing process are balanced by changing the pressure and spindle speed, and then the optimal surface roughness is obtained. During the experiment, six groups of different pressures and spindle speeds were set up. HASS-VF-3 equipment was used to uniformly polish the aluminum alloy mirror, and the polishing results were detected by Zygo's New View 7200 white light interferometer. Each group of experiments was carried out twice. After each polishing, the average surface roughness was measured at 6~8 points, and the surface roughness range was marked. The polishing process and detection process are shown in Fig. 12.

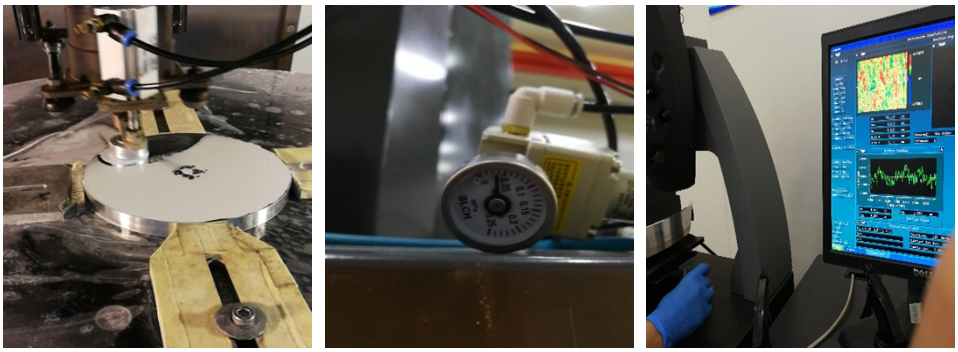

(a) (b) (c)

Fig. 12. Aluminum alloy mirror processing and testing process. (a) Polishing process; (b) Pressure setting process; (c) Detection process.

The setting of the polishing pressure is shown in Table 4 When the polishing pressure is changed, the spindle speed is set to 300 r/min. The polishing results are shown in Fig. 13.

Optics EXPRESS

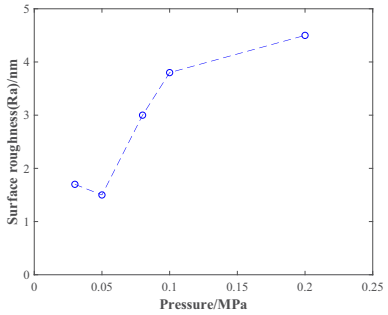

Fig. 13. Polishing results under different pressures.

Table 4. Setting of polishing pressure

Number	Pressure/MPa	*Ra*/nm
1	0.03	1.7±0.2
2	0.05	1.5±0.2
3	0.08	3±0.2
4	0.1	3.8±0.2
5	0.2	4.5±0.2
6	0.3	Scratch obvious

It can be seen from Fig. 13 that with an increase in pressure, the surface roughness of the aluminum alloy mirror decreases first and then increases. When the pressure is less than 0.05 MPa, the surface roughness decreases with increasing pressure, which is because the pressure is too small. The abrasive particles cannot be completely pressed into the aluminum alloy surface, resulting in incomplete removal of material. When the applied pressure is 0.05 MPa, the minimum surface roughness *Ra* is 1.5 nm. When the applied force is greater than 0.05 MPa, the surface roughness increases with increasing pressure. When the pressure is 0.3 MPa, the polishing surface has obvious scratches. Therefore, the most suitable polishing pressure for aluminum alloy mirrors is 0.05 MPa.

The setting of the spindle speed is shown in Table 5. When the spindle speed is changed, the polishing pressure is set to 0.05 MPa. The polishing results are shown in Fig. 14.

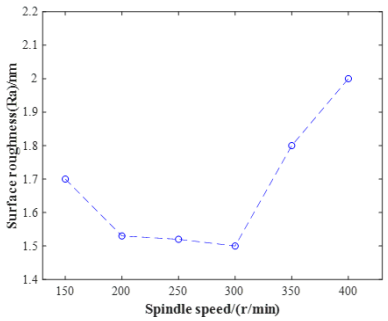

Fig. 14. Polishing results at different spindle speeds.

It can be seen from Fig. 14 that with the increase of spindle speed, the surface roughness of the aluminum alloy mirror decreases first and then increases. When the spindle speed is less than

Optics EXPRESS

Table 5. Setting of spindle speed

Number	Spindle speed/(r/min)	Ra/nm
1	150	1.7±0.2
2	200	1.53±0.2
3	250	1.52±0.2
4	300	1.5±0.2
5	350	1.8±0.2
6	400	2±0.2

300 r/min, the surface roughness decreases with the increase of the spindle speed. When the spindle speed is greater than 300 r/min, the surface roughness increases with increasing spindle speed. In the experiment, it was found that the surface roughness of the aluminum alloy mirror changed little when the polishing speed was 200 r/min~300 r/min, and the polishing efficiency at 300 r/min was greater than that at 200 r/min. Therefore, the most suitable spindle speed for polishing aluminum alloy mirror is 300 r/min.

3.3.2. Polishing experiments and results

The whole process flow of aluminum alloy mirror processing and the expected processing indexes of each stage are shown in Fig. 15.

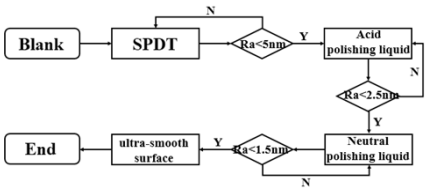

Fig. 15. Processing flow of an aluminum alloy mirror.

Through the above analysis, the polishing parameters shown in Table 6 are used to quickly and uniformly polish the aluminum alloy mirror after SPDT processing.

Table 6. Polishing parameters

Pressure	Revolution Speed	Grinding head size	Tool head eccentricity	Abrasive materials	Grain diameter	Polishing pad
0.05MPa	300r/min	30mm	5mm	AlCeH3O3	0.8μm	Damping flannel

Firstly, the high-efficiency acidic polishing liquid is used to quickly polish the aluminum alloy mirror. Through the chemical reaction between the acidic liquid and the RSA-6061 aluminum alloy mirror, the purpose of quickly removing the turning texture and reducing surface roughness is realized. Then, the RSA-6061 aluminum alloy mirror polished with the acid polishing liquid is polished with the neutral polishing liquid. The results of each polishing stage are shown in Fig. 16.

It can be seen from Fig. 16 that the slope of the surface roughness decline curve when polishing with acidic polishing liquid is significantly larger than that when polishing with neutral polishing liquid, that is, acidic polishing liquid has higher removal efficiency. And the surface roughness *Ra* of the RSA-6061 aluminum alloy mirror has been reduced to 2.402 nm after polishing with high-efficiency acid polishing liquid for 1 h. It can be seen that the special acidic polishing liquid can realize the rapid removal of turning texture, but there are still surface defects (pits) on the

Optics EXPRESS

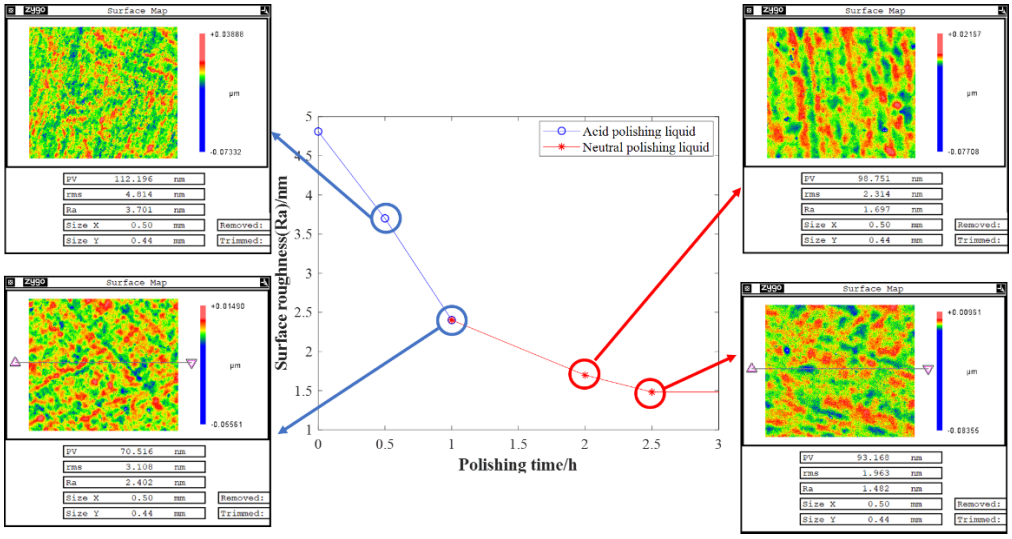

Fig. 16. Polishing results at different times.

surface of the aluminum alloy mirror. Due to the existence of these surface defects, the aluminum alloy mirror still has high-frequency errors. To remove surface defects, reduce surface roughness, and suppress the high-frequency error of the aluminum alloy mirror, we used the prepared neutral polishing liquid to polish the aluminum alloy mirror for 1.5 h. The polishing results are shown in Fig. 16, the final surface roughness *Ra* value of the RSA-6061 aluminum alloy mirror is reduced to 1.482 nm. In summary, after 2.5 h of high-efficiency polishing of aluminum alloy mirror using a combination of high-efficiency acid polishing liquid and neutral polishing liquid, the surface roughness *Ra* decreased from 4.811 to 1.482 nm. Therefore, the combination of high-efficiency acidic polishing liquid and neutral polishing liquid can greatly improve polishing efficiency and reduce surface roughness.

The RSA-6061 aluminum alloy plane mirror polished by the combination of high-efficiency acid polishing liquid and neutral polishing liquid is shown in Fig. 17.

Through the experimental results after polishing in Fig. 17(b), it can be seen that the surface defects (pits) have been removed and the remaining surface defects can be considered as surface defects caused by the defects of the material itself. And through Fig. 17(c), it can be seen that the RMS of the surface profile accuracy after polishing is 13.306 nm, which is 41.25% higher than the turning result (RMS value is 22.65 nm). Therefore, small tool polishing does not expand the surface accuracy error.

To verify the ability of small tool polishing to suppress the high-frequency of the aluminum mirror surface processed by SPDT, power spectral density (PSD) analysis was introduced to visualize the spatial frequency. Fig. 18 reflects the suppression effect of small tool polishing on SPDT high-frequency error.

The frequency error PSD curves of the aluminum alloy mirror after SPDT and polishing are compared and analyzed. The results are shown in Fig. 18. Small tool polishing can be found to have greatly improved the frequency error of the aluminum alloy mirror, especially in the range of 0.5~2mm^{-1}, the improvement effect is very obvious, and the amplitude of the PSD curve decreases greatly. Therefore, polishing with a small tool can quickly and efficiently remove the turning texture of diamond turning, suppress the medium and high-frequency errors of aluminum alloy mirrors, and obtain aluminum alloy mirrors with high surface quality and ultra-smooth surface that can be directly applied to visible light systems.

Optics EXPRESS

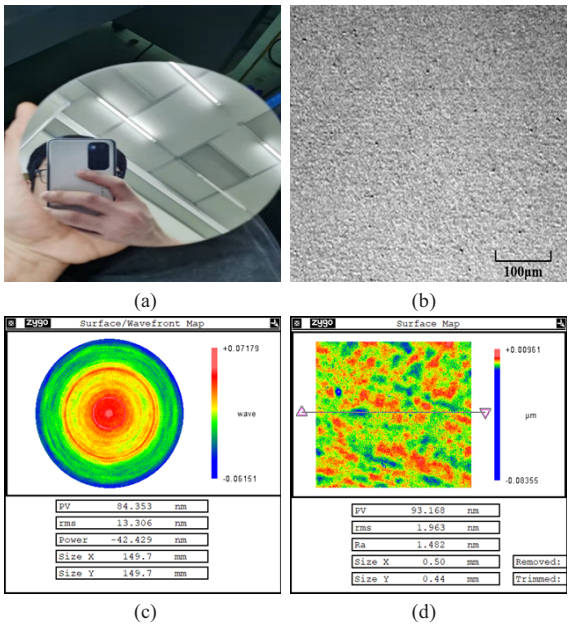

Fig. 17. Aluminum alloy plane mirror. (a) Object diagram; (b) Images under a high power microscope; (c) Surface profile test results after polishing; (d) Surface roughness test results after polishing.

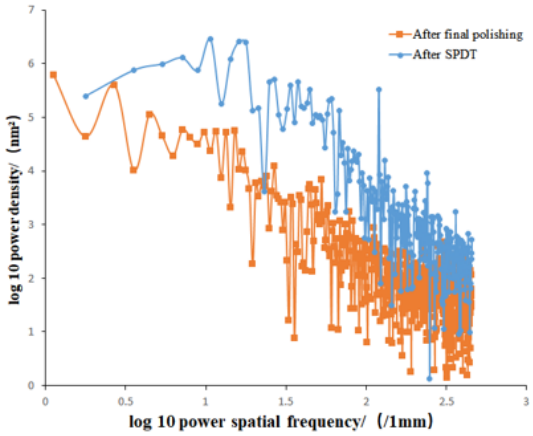

Fig. 18. Comparison of PSD curves after single point diamond turning and polishing.

In summary, for the processing of aluminum alloy mirrors used in visible-light systems, we optimize the processing strategy as follows. Firstly, the surface roughness is rapidly reduced by single point diamond turning. Then, for the single point diamond turning texture, a small tool polishing combined with an acidic polishing liquid is used to quickly polish the turning texture of the aluminum alloy mirror to reduce surface roughness. Finally, the aluminum alloy mirror is finely polished with a neutral polishing liquid to obtain an ultra-smooth aluminum alloy surface after removing surface defects (pits). This method can reduce the limitation of the use of aluminum alloy mirrors in visible light optical systems due to turning texture and surface roughness.

Optics EXPRESS

4. Conclusions

In this paper, an optimized processing method combining single point diamond turning and small tool polishing is proposed to improve the surface quality of aluminum alloy mirrors. Firstly, the single point diamond turning technology is used to quickly obtain the surface of nanoscale roughness aluminum alloy mirror. After that, the small tool polishing method is used to remove the turning texture on the surface of the aluminum alloy mirror, reduce surface roughness, suppress medium and high-frequency errors on the surface, and further improve surface quality. The main conclusions are as follows:

1. The mapping relationship between surface roughness and turning parameters was established. By controlling the turning parameters, the aluminum alloy mirror with surface roughness *Ra* less than 5 nm can be quickly obtained by single point diamond turning. However, because of the existence of turning texture on the surface, the use of the mirror was limited.

2. To improve the polishing accuracy of small tool polishing and ensure processing efficiency. The effects of different polishing pressures and speeds on the material removal efficiency were predicted by numerical simulation. According to the chemical composition of the aluminum alloy material, two types of acidic and neutral polishing liquids were prepared. Through theoretical analysis, it has been proved that small tool polishing can quickly reduce the surface roughness of aluminum alloy mirrors. Taking the aluminum alloy plane mirror with an aperture of 150 mm as an example, the optimized processing method proposed in this paper was applied to the process. After measurement, the surface roughness *Ra* decreased from 4.81 nm to 1.48 nm, an increase of 69.2%.

The experimental results show that the processing method proposed in this paper can effectively improve the surface quality of aluminum alloy mirrors, and lay a foundation for its application in the visible light band.

Funding. National Key Research and Development Program of China (2022YFC2203902); National Natural Science Foundation of China (12203048).

Acknowledgments. Authors thank Prof. Yang for her academic guidance and Prof. Bai for his help in the experiments.

Disclosures. The authors declare no conflicts of interest.

Data availability. Data underlying the results presented in this paper are not publicly available at this time but may be obtained from the authors upon reasonable request.

References

1. G. Willers, C. Hagendorf, V. Naumann, R. Holzlöhner, and S. Guisard, "Soiling induced nano-defects on aluminum telescope mirror coatings," Appl. Opt. **61**(10), 2727–2732 (2022).
2. B. Chen, X. Zhang, and L. He, "Solar X-ray and EUV imager on board the FY-3E satellite," Light: Sci. Appl. **11**(1), 329 (2022).
3. L. Yan, X. Zhang, Q. Fu, L. Wang, G. Shi, S. Tan, K. Zhang, and M. Liu, "Assembly-level topology optimization and additive manufacturing of aluminum alloy primary mirrors," Opt. Express **30**(4), 6258–6273 (2022).
4. P. Chioetto, P. Zuppella, and V. D. Deppo, "Qualification of the thermal stabilization, polishing and coating procedures for the aluminum telescope mirrors of the ARIEL mission," Exp. Astron **53**(2), 885–904 (2022).
5. Y. Bai, X. Zhang, C. Yang, L. Li, and X. Luo, "Material removal model of magnetorheological finishing based on dense granular flow theory," Light: Adv. Manuf. **3**(4), 1–10 (2022).
6. J. Guo, C. Yang, C. Xue, and P. Song, "Material removal mechanism and MR fluid for magnetorheological finishing of an RSA-6061 aluminum alloy mirror," Appl. Opt. **61**(34), 10098–10104 (2022).
7. Y. Huang, B. Fan, Y. Wan, and S. Li, "Improving the performance of single point diamond turning surface with ion beam figuring," Optik **172**, 540–544 (2018).
8. L. Zhu, Y. Zhang, and H. Sun, "Miniaturising artificial compound eyes based on advanced micronanofabrication techniques," Light: Adv. Manuf. **2**(1), 84–100 (2021).
9. Z. Geng, Z. Tong, and X. Jiang, "Review of geometric error measurement and compensation techniques of ultra-precision machine tools," Light: Adv. Manuf. **2**(2), 211–227 (2021).

Optics EXPRESS

10. T. Sugano, K. Takeuchi, T. Goto, Y. Yoshida, and N. Ikawa, "Diamond turning of an aluminum alloy for mirror," CIRP Ann. **36**(1), 17–20 (1987).
11. A. Sharma, D. Datta, and R. Balasubramaniam, "A molecular dynamics simulation of wear mechanism of diamond tool in nanoscale cutting of copper beryllium," Int. J. Adv. Manuf. Technol. **102**(1-4), 731–745 (2019).
12. S. Zhang, J. Yu, S. To, and Z. Xiong, "A theoretical and experimental study of spindle imbalance induced forced vibration and its effect on surface generation in diamond turning," Int. J. Mach. Tools Manuf. **133**, 61–71 (2018).
13. H. Cheng, Z. Dong, X. Ye, and H. Tam, "Subsurface damages of fused silica developed during deterministic small tool polishing," Opt. Express **22**(15), 18588–18603 (2014).
14. W. Cho, Y. Ahn, C. Baek, and Y. Kim, "Effect of mechanical process parameters on chemical mechanical polishing of Al thin films," Microelectron. Eng. **65**(1-2), 13–23 (2003).
15. A. Yoomin, J. Yoon, C. K. Baek, and Y. Kim, "Chemical mechanical polishing by colloidal silica-based slurry for micro-scratch reduction," Wear **257**(7-8), 785–789 (2004).
16. C. Du, Y. Dai, C. Guan, and H. Hu, "High efficiency removal of single point diamond turning marks on aluminum surface by combination of ion beam sputtering and smoothing polishing," Opt. Express **29**(3), 3738–3753 (2021).
17. T. Zhao, H. Hu, X. Peng, C. Du, C. Guan, and J. Yong, "Study on the surface crystallization mechanism and inhibition method in the CMP process of aluminum alloy mirrors," Appl. Opt. **58**(22), 6091–6097 (2019).
18. B. Sui, F. Huo, C. Li, C. Yang, and C. Xue, "Ultra-Precision Turning Process and Optimization of Infrared Diffraction Optical Mold Insert," Acta Opt. Sin. **42**(13), 1312004 (2022).
19. R. Jasinevicius, J. Otoboni, I. Basso, and M. Dib, "Size effects in ultraprecision machining of aluminum alloys: Conventional aa6061-t6 and rsa 6061-t6," J. Manuf. Process. **68**, 136–157 (2021).
20. N. Khatri, B. Barkachary, B. Muneeswaran, R. Al-Sayegh, X. Luo, and S. Goel, "Surface defects incorporated diamond machining of silicon," Int. J. Extrem. Manuf. **2**(4), 045102 (2020).
21. C. He, W. Zong, and T. Sun, "Origins for the size effect of surface roughness in diamond turning," Int. J. Mach. Tools Manuf. **106**, 22–42 (2016).
22. Z. Geng, N. Huang, M. Castelli, and F. Fang, "Polishing Approaches at Atomic and Close-to-Atomic Scale," Micromachines **14**(2), 343 (2023).
23. J. Guo, X. Shi, C. Song, L. Niu, H. Cui, X. Guo, Z. Tong, N. Yu, Z. Jin, and R. Kang, "Theoretical and experimental investigation of chemical mechanical polishing of W-Ni-Fe alloy," Int. J. Extrem. Manuf. **3**(2), 025103 (2021).
24. D. Liu, G. Chen, and Q. Hu, "Material removal mechanism and material removal rate model of polishing process for quartz glass using soft particle," SPIE **9633**, 58–73 (2015).
25. X. Chen, Y. Zhao, and Y. Wang, "Modeling the effects of particle deformation in chemical mechanical polishing," Appl. Surf. Sci. **258**(22), 8469–8474 (2012).
26. E. Rabinowicz, *Friction and Wear of Materials*, 2nd Edition. (Wiley: New York) (1995).
27. Y. Jeng and P. Huang, "Impact of abrasive particles on the material removal rate in CMP: A microcontact perspective," Electrochem. Solid-State Lett. **7**(2), G40 (2004).